Full Paper

Propellants, Explosives, Pyrotechnics

DOI: 10.1002/prep.201600073

Blast Waves and Fragment Velocities of Erythritol Tetranitrate

Masahiro Tagawa,*[a] Reiko I. Hiyoshi,[a] Masaru Takeuchi,[a] and Kimiya Akita[a]

Abstract: Erythritol tetranitrate (ETN) is a highly sensitive nitrate ester that has a molecular structure similar to nitroglycerine and pentaerythritol tetranitrate (PETN). In this study, experiments detonating 175 g of ETN were repeated three times to measure blast waves 0.6 m above the ground. TNT and PETN were also tested under the same conditions for comparison. The average peak overpressure of ETN was about 30 kPa at 3 m from the explosion center (5.4 m kg$^{-1/3}$ scaled distance), which was much higher than that of TNT (about 22 kPa) and similar to PETN. The effects of the reflected wave from the ground appeared at greater distances of 5 and 7 m (8.9 and 12.5 m kg$^{-1/3}$, respectively), as verified by the waveforms and high-speed camera images. Previous TNT data for peak overpressure vs. scaled distance were used to calculate the TNT equivalents for the experimental data, which revealed that ETN had a similar value to PETN. The fragment velocities of steel cylinders were measured, and that of ETN (1040 m s^{-1}) was higher than that of TNT (957 m s^{-1}) and lower than that of PETN (1260 m s^{-1}). The Gurney constant for each explosive was obtained by using the initial fragment velocities.

Keywords: Erythritol tetranitrate · TNT equivalent · Mach reflection · Metal fragments · Gurney constant

1 Introduction

Erythritol tetranitrate (ETN) (Figure 1) is a simple nitrate ester that was first prepared in 1949 by Stenhouse [1], although it has not been investigated as an explosive until recently. There is increasing concern that ETN will become a common home-made explosive (HME) owing to its relatively easy synthesis and the increased availability of erythritol, the starting material for ETN [2–4]. ETN is more sensitive than pentaerythritol tetranitrate (PETN), but less sensitive than nitroglycerin [5,6]. The high sensitivity of ETN means that it must be handled with the utmost care [2,6,7]. The crystal structure, physical and chemical properties of ETN have been reported recently, and its similarity to PETN was highlighted [2,6,8], although they have different melting points and oxygen balances [5].

Recently, Manner et al. reported the detonation velocity and critical diameter of ETN, suggesting that its high explosive performance is similar to PETN [8]. However, the explosion properties of ETN have not been thoroughly investigated. The pressure of blast waves and fragment velocities generated by ETN, especially for large charges, are not known.

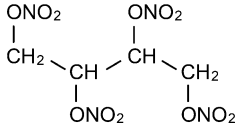

Figure 1. Molecule of erythritol tetranitrate.

In the presented study, several hundred grams of ETN was prepared and explosion experiments were conducted. Blast parameters, such as peak overpressure and impulse, from ETN were measured and compared with those of TNT and PETN. To date, a huge amount of data has been published about TNT on the relationships between peak overpressure and scaled distance, and the scaled impulse and scaled distance. These correlations were summarized in the peak overpressure/scaled impulse vs. scaled distance curves, referred to as the standard curves [9–13]. These standard curves for TNT differ from each other owing to the different experimental conditions, such as whether the explosions were measured in air, or on or above the ground. The standard curves for the explosion in air consisted of only the incident wave, whereas the curves for on or above the ground include the effect of the reflected wave from the ground. We performed experiments 0.6 m above the ground at the height our former data were measured [13]. We also compared the peak overpressures and scaled distances with standard curves reported by Baker [9], and reported as the MITI87 [12] and NRIPS09 [13] curves. In addition, the fragment velocities of steel cylinders

[a] *M. Tagawa, R. I. Hiyoshi, M. Takeuchi, K. Akita*
Explosion Investigation Section
Second Department of Forensic Science
National Research Institute of Police Science
6-3-1 Kashiwanoha, Kashiwa, Chiba, Japan
**e-mail: tagawa@nrips.go.jp*

filled with TNT, ETN, and PETN were measured. Gurney constants of these explosives were calculated by using the initial fragment velocity [14,15].

2 Experimental Section

2.1 Preparation of Explosives

The explosives used in this study are summarized in Table 1. TNT was purchased from Chugoku Kayaku Co., Ltd. and PETN from Kayaku Japan Co., Ltd. TNT were prepared by passing crystalline TNT through a 1.2 mm sieve. ETN was synthesized according to the mixed acid method reported by Oxley et al. [5] and recrystallized according to the literature [6]. ETN was identified by GC/MS by comparing the retention time and mass spectroscopic data with reference standards (AccuStandard Inc.). ETN was kept wet until it was used because dry ETN is very sensitive.

2.2 Blast Wave Measurement

Blast wave measurements were repeated three times with ETN (175 g). The same measurements were done with TNT and PETN separately, although the PETN amount used was 150 g instead of 175 g for one measurement. Composition C-4 (2 g) was used as a booster for TNT (Table 1). Explosives were loaded into a paper tube (diameter: 68 mm) and placed on top of timbers at a height of 0.6 m. A No. 6 electric detonator (Kayaku Japan Co., Ltd) was placed on the top of the explosive charge. The pressure values of the blast wave were measured with pressure sensors (137A23, PCB Piezotoronics Inc.) placed 3, 5, and 7 m from the explosion center and 0.6 m above the ground, which was the same height as the explosive charges. Two sensors were used at each distance. Blast pressure data were recorded by oscilloscopes at a frequency of 500 MHz, as mentioned in Ref. [16].

2.3 Obtaining Blast Wave Parameters and Comparing with Previous Data

The peak overpressure and the positive phase impulse were obtained by applying Sachs' scaling law and converted into the values for 0 m above sea level of 101.325 kPa and 288.15 K, as described by Matsunaga et al. [17,18]. The best fitting exponential curve for the overpressure was plotted to determine the peak overpressure values, as reported by Arai et al. [13]. The MITI87 standard curve was obtained by TNT explosions at a scaled distance from 1.4 to 21.5 m kg$^{-1/3}$, and with scaled height of 0.18 m kg$^{-1/3}$. The NRIPS09 standard curve was obtained by TNT explosions at a scaled distance from 1.4 to 31 m kg$^{-1/3}$, and a scaled height of 0.22 to 0.70 m kg$^{-1/3}$. The MITI87 standard curve was expressed as polynomial functions of the scaled distance in any range, and it was used to estimate TNT equivalents in this study. In addition, the ratio of the peak overpressure against the MITI87 curve (P_{exp}/P_{MITI87}), and the ratio of the scaled impulse against the MITI87 curve (I_{exp}/I_{MITI87}) were also calculated. The ratios were obtained by using experimental data (P_{exp} or I_{exp}) and values derived from MITI87 functions at the corresponding scaled distance (P_{MITI87} or I_{MITI87}) and averaging. Because the scaled distances were from 5.33 to 13.2 m kg$^{-1/3}$ in this study, MITI87 functions with a range of $4.30 < Z < 6.81$, $6.81 < Z < 10.80$, and $10.80 < Z < 17.11$ were used, where Z is the scaled distance.

2.4 Visualization of Shock Front by using High-speed Camera Images

High-speed camera images of the explosions were recorded at 22,002 frames per second (fps) in the blast wave experiments by Phantom V2010 (Vision Research Inc.). The distance from the explosion center to the camera was about 50 m. The experiment was performed with 175 g of TNT without pressure sensors. To help visualize the shock front, a checked cloth was placed behind the explosion site. Camera images were edited to clarify the shock front according to Kudo et al. and Leete et al. [19,20] by using software (Photoshop Elements 10, Adobe). The differences between two adjacent frames were subtracted, and the gamma values and white balances were adjusted. The distance in the images was calculated by software (Pixel Runner, TellusImage, Co., Ltd.).

2.5 Fragment Velocity Measurement

Seamless steel pipe was used as a cylindrical container (inner diameter: 54.1 mm; thickness: 3.2 mm; height:

Table 1. Explosives and casings used in this study.[a)]

Experiment	TNT	ETN	PETN
Blast wave measurement	Three replicates of 175 g (2 g Composition C-4), $\rho \approx 0.83$ g cm^{-3}	Three replicates of 175 g, $\rho \approx 0.73$ g cm^{-3}	Two replicates of 175 g and one replicate of 150 g, $\rho \approx 0.87$ g cm^{-3}
Fragment velocity measurement	$C = 99$ g, $M = 229$ g, $C/M = 0.43$, $\rho = 0.86$ g cm^{-3}	$C = 81$ g, $M = 229$ g, $C/M = 0.35$, $\rho = 0.71$ g/cm^3	$C = 101$ g, $M = 229$ g, $C/M = 0.44$, $\rho = 0.88$ g cm^{-3}
	$C = 94$ g, $M = 228$ g, $C/M = 0.41$, $\rho = 0.81$ g cm^{-3}	C = 84 g, M = 230 g, $C/M = 0.37$, $\rho = 0.73$ g cm^{-3}	$C = 103$ g, $M = 227$ g, $C/M = 0.45$, $\rho = 0.89$ g cm^{-3}

a) All explosives were in powder form, and ρ is the loaded density of the explosive. The capital letters C and M represent the mass of the explosives and metal casings in the fragment velocity experiment, respectively.

DOI: 10.1002/prep.201600073

50 mm), the bottom of which was covered with cardboard. Explosives and the steel casings are detailed in Table 1. The explosive in the steel cylinder was placed on top of timber at a height of 0.6 m, and initiated from the top surface by a No. 6 electric detonator. This experiment was repeated twice for the three kinds of explosives.

Three pairs of steel plates (0.6 mm thick) were placed upright at 0.5, 1.0, and 2.0 m from the explosive to visualize the impact of fragments. High-speed camera images were recorded at 35,000 fps. Fragment velocities were measured by sensors consisting of insulated two pieces of aluminum foil with an electrical circuit attached to the back surface of the steel plates. The fragment velocities were calculated from the arrival times and distances, and the initial velocities were obtained from the average of the data measured at 0.5 m.

3 Results

3.1 Blast Wave Parameters and Waveforms

In the blast wave measurements, pressure vs. time was recorded. Blast data were summarized in the peak overpressure and positive phase impulse. The waveform of the TNT explosion at 3 m shows the second (reflected) wave after the arrival of the incident wave (Figure 2a). In contrast, this reflected wave was not observed in the waveforms at 5 m (Figure 3a) and 7 m, and only one peak was observed. There were no significant differences in the waveforms of ETN and PETN compared with TNT, except that the time intervals between the first and second waves of ETN and PETN were shorter than for TNT (Figure 2 and Figure 3). The peak overpressures of ETN (P_{ETN}) and PETN (P_{PETN}) were higher than that of TNT (P_{TNT}), and the arrival time of the shock waves of ETN and PETN were earlier than that of TNT (Figure 2 and Figure 3). As was observed for peak overpressure, the scaled impulses of ETN (I_{ETN}) and PETN (I_{PETN}) were higher than that of TNT (I_{TNT}).

To verify how the blast wave propagated in air and was reflected from the ground, high-speed camera images were analyzed. Under these experimental conditions, the Mach stem was formed. When the first wave reached the sensor 3 m from the explosion center, the triple point had risen from ground level, although the height was still below the height of the sensor (Figure 4).

3.2 Comparison with Previous TNT Blast Data

The relationships of peak overpressure vs. scaled distance and scaled impulse vs. scaled distance are well established, and there is a long history of using TNT as a standard to compare or estimate the performance of explosives. These correlations are summarized in standard curves. In this article, two standard TNT curves are used: a curve based on explosions in air (Baker) [9], and curves based on explosions above the ground surface (MITI87 and NRIPS09) [12, 13],

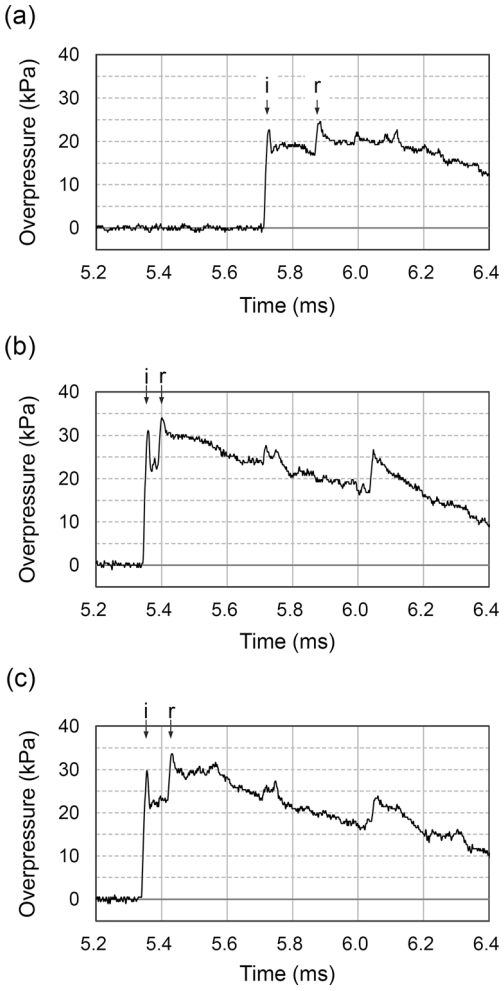

Figure 2. Blast waveforms of (a) TNT, (b) ETN, and (c) PETN at 3 m are shown. Two arrows labeled "i" and "r" indicate the arrival times of the first (incident) wave and the second (reflected) wave.

because the effect of the reflected waves depended on the distance as described in previous section.

P_{TNT} at 3 m was close to the Baker curve, whereas P_{TNT} at 5 and 7 m were close to the MITI87 curve (Figure 5). At any scaled distances, P_{ETN} were higher than P_{TNT}, and were similar to P_{PETN}. The ratio of peak overpressure to MITI87 (P_{exp}/P_{MITI87}) was calculated for each explosive. The values of P_{ETN}/P_{MITI87} (1.25 at 5 m and 1.19 at 7 m) and P_{PETN}/P_{MITI87} (1.24 at 5 m and 1.18 at 7 m) indicated that there were no big differences between ETN and PETN in the peak overpressure (Table 2). TNT equivalent values were obtained from the data at 5 and 7 m against the MITI87 curve. The average TNT equivalents were 1.57 for ETN and 1.54 for PETN against the MITI87 curve under these experimental conditions, where that of TNT taken as 1.00.

The scaled impulse of TNT (I_{TNT}) at 3 m was smaller than that of the MITI87 curve, and I_{TNT} at 5 and 7 m were larger than the MITI87 curve (Figure 6). For the scaled impulse, the MITI87 curve was the most similar at any distance. The

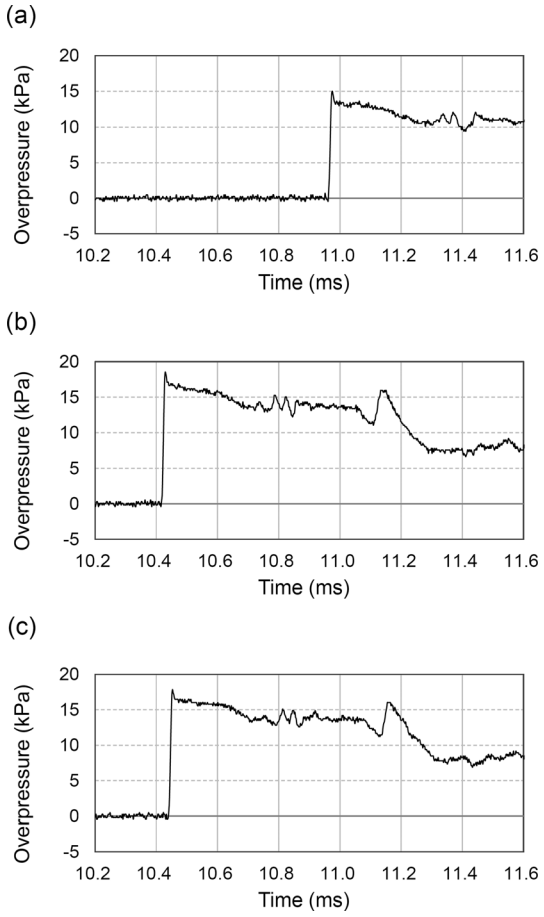

Figure 3. Blast waveforms of (a) TNT, (b) ETN, and (c) PETN at 5 m.

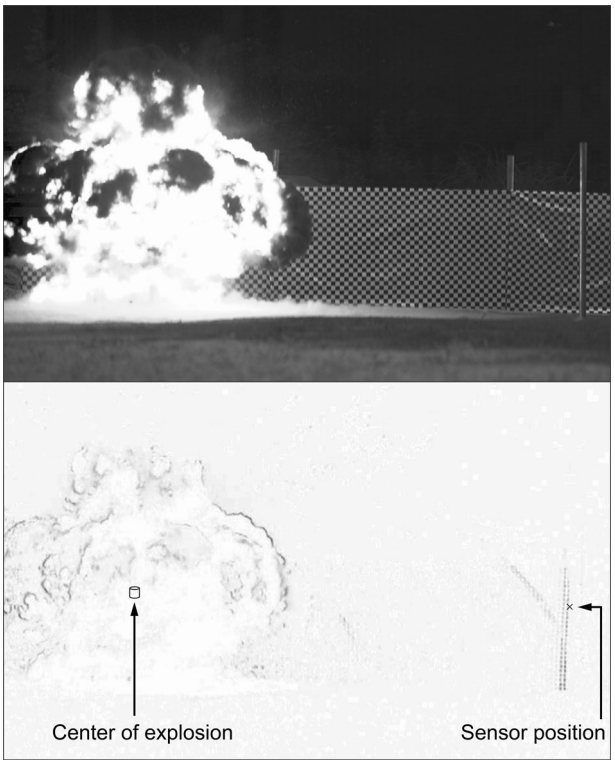

Figure 4. Images from the high-speed camera of the explosion of 175 g TNT obtained 5.3 ms after initiation. The bottom image is processed to visualize the shock front. The cylinder represents the center of explosion (0.6 m above the ground) and the cross represents the position of the pressure sensor 3 m from the explosion center at a height of 0.6 m.

values of I_{ETN}/I_{MITI87} (1.38 at 5 m and 1.27 at 7 m) were slightly smaller than the values of I_{PETN}/I_{MITI87} (1.45 at 5 m and 1.34 at 7 m) (Table 2).

3.3 Fragment Velocity

The fragment velocities of the steel cylinder were calculated by using the distance to the foil sensor and the arrival

Table 2. Ratio of peak overpressure and scaled impulse against MITI87 for each explosive.[a)]

	Ratio of peak overpressure and scaled impulse against MITI87								
	3 m			5 m			7 m		
	Scaled distance [m kg$^{-1/3}$]	P_{exp}/P_{MITI87}	I_{exp}/I_{MITI87}	Scaled distance [m kg$^{-1/3}$]	P_{exp}/P_{MITI87}	I_{exp}/I_{MITI87}	Scaled distance [m kg$^{-1/3}$]	P_{exp}/P_{MITI87}	I_{exp}/I_{MITI87}
TNT	5.34	0.72	1.17	8.90	1.02	1.08	12.38	0.89	0.95
	5.35	0.71	1.16	8.89	1.02	1.09	12.38	0.98	0.97
	5.34	0.70	1.17	8.90	1.03	1.08	12.38	0.91	0.97
	5.43	0.61	0.94	8.97	1.00	1.11	12.51	1.03	1.04
	5.43	0.62	0.93	8.96	1.05	1.11	12.50	1.01	1.04
	5.43	0.58	0.91	8.97	1.02	1.10	12.52	1.05	1.04
Average		**0.66**	**1.05**		**1.02**	**1.09**		**0.98**	**1.00**
ETN	5.36	0.85	1.48	8.92	1.25	1.34	12.43	1.13	1.22
	5.38	0.83	1.50	8.94	1.22	1.35	12.44	1.14	1.23
	5.33	1.00	1.48	8.89	1.23	1.35	12.38	1.13	1.20
	5.45	0.92	1.18	9.00	1.25	1.41	12.57	1.25	1.33
	5.45	1.03	1.17	9.01	1.26	1.41	12.58	1.25	1.34
	5.50	0.91	1.16	9.04	1.27	1.42	12.60	1.26	1.33
Average		**0.92**	**1.33**		**1.25**	**1.38**		**1.19**	**1.27**

DOI: 10.1002/prep.201600073

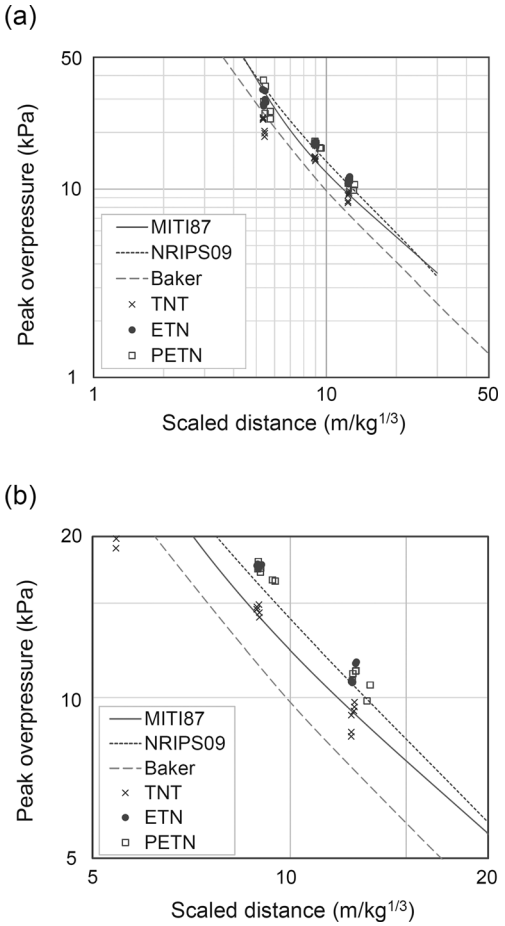

Figure 5. Peak overpressure vs. the scaled distance of standard curves and experimental data for TNT, ETN, and PETN. Standard curves for the air explosion (Baker) and the above-ground explosion (MITI87 and NRIPS09) of TNT are shown as lines. The peak overpressure of TNT, ETN, and PETN at distances of 3, 5, and 7 m are plotted. (a) All experimental data and (b) an expanded view of (a).

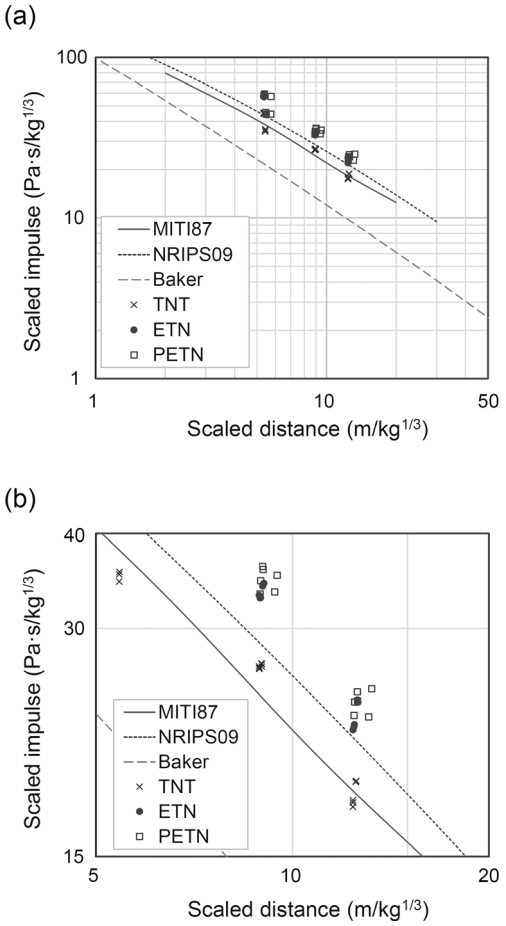

Figure 6. Scaled impulse vs. the scaled distance of standard curves and experimental data of TNT, ETN, and PETN. Standard curves for the air explosion (Baker) and above-ground explosion (MITI87 and NRIPS09) of TNT are shown as lines. The scaled impulse of TNT, ETN, and PETN at distances of 3, 5, and 7 m are plotted. (a) All experimental data and (b) an expanded view of (a).

time (Figure 7). The velocities decreased as the distance increased, and the slopes of the fitted curve became gradual. As for the initial velocity (V_0), PETN (1260 m s^{-1}) was the fastest, ETN (1040 m s^{-1}) came in second, and TNT

Table 2. (Continued)

	Ratio of peak overpressure and scaled impulse against MITI87								
	3 m			5 m			7 m		
	Scaled distance [m kg$^{-1/3}$]	P_{exp}/P_{MITI87}	I_{exp}/I_{MITI87}	Scaled distance [m kg$^{-1/3}$]	P_{exp}/P_{MITI87}	I_{exp}/I_{MITI87}	Scaled distance [m kg$^{-1/3}$]	P_{exp}/P_{MITI87}	I_{exp}/I_{MITI87}
PETN	5.38	0.88	1.54	8.94	1.26	1.42	12.45	1.18	1.32
	5.36	1.13	1.51	8.92	1.22	1.36	12.43	1.14	1.26
	5.75	0.89	1.58	9.39	1.25	1.44	13.08	1.11	1.31
	5.45	0.78	1.20	9.00	1.22	1.49	12.57	1.21	1.37
	5.47	1.09	1.17	9.02	1.24	1.48	12.58	1.21	1.33
	5.74	0.81	1.22	9.48	1.26	1.52	13.23	1.20	1.44
Average		**0.93**	**1.37**		**1.24**	**1.45**		**1.18**	**1.34**

a) The ratio of the peak overpressure and scaled impulse against MITI87 are shown. The ratios were obtained from the experimental data (P_{exp} or I_{exp}) and values were derived from MITI87 functions at the corresponding scaled distance (P_{MITI87} or I_{MITI87}). The average values are shown in bold type.

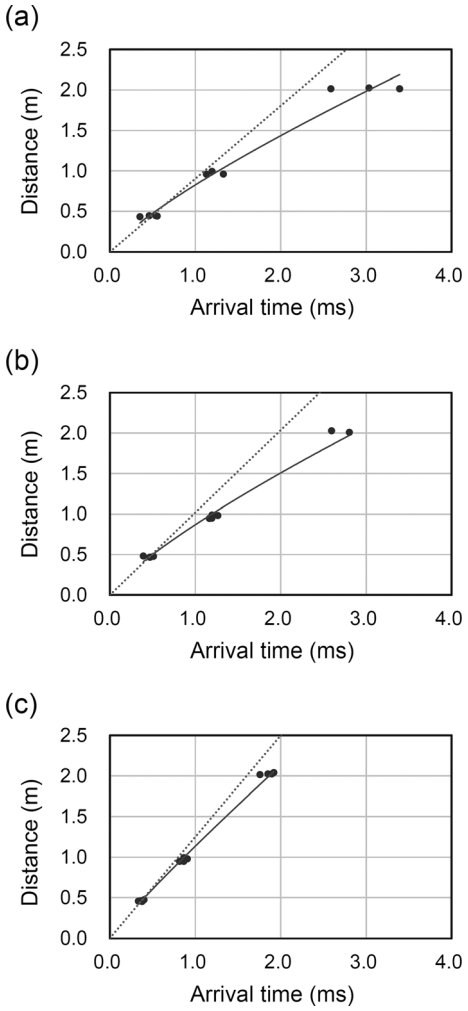

Figure 7. The fragment velocities of (a) TNT, (b) ETN, and (c) PETN. The curved lines indicate the approximate curves and the slopes of the dotted straight line indicate the initial velocities (V_0) obtained at 0.5 m.

(957 m s^{-1}) was the slowest. Unlike the peak overpressure, V_0 of ETN and PETN were significantly different. By applying the V_0 to the Gurney equation, the Gurney constant was obtained, which was 1.63 km s^{-1} for TNT, 1.88 km s^{-1} for ETN, and 2.08 km s^{-1} for PETN. The high-speed camera images showed bright sparks at the moment of fragment impact on the steel plates (Figure 8). The numbers of through-holes in the 0.6-mm-thick steel plates were counted. PETN made the most holes, followed by ETN and TNT (Table 3), which was the same order as the initial fragment velocities (V_0).

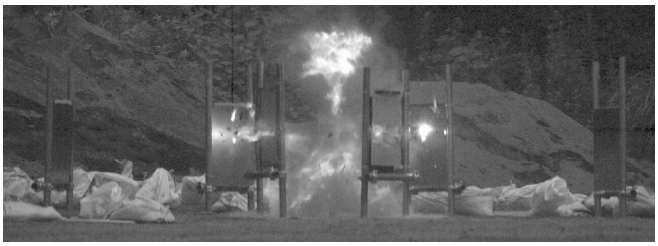

Figure 8. Image of ETN explosion obtained 1.2 ms after ignition. The moment that metal fragments hit the steel plates is shown. Bright sparks are observed after the impact.

4 Discussion

In this study, ETN blast wave parameters were compared with those of TNT and PETN, the peak overpressure was compared with standard curves of TNT (Baker, MITI87, and NRIPS09), and the TNT equivalent for each explosive was obtained. The effect of the reflected wave on the peak overpressure was identified; therefore, the waveforms and the Mach stem position were evaluated carefully [20, 21]. Figure 4 shows that the height of the triple point was still below 0.6 m, where the pressure sensor was placed; therefore, the incident and reflected waves were separately recorded by the sensor at 3 m (Figure 2). The peak overpressure values at 3 m were obtained by using only the incident waveform, so these data excluded the effect of the reflected wave. Thus, the value was close to the air explosion data in the Baker curve. In contrast, at 5 and 7 m, the height of the triple point increased and exceeded the height of the sensor, and then the Mach stem reached the sensor, and hence there were no notable peaks after the first wave at 5 m (Figure 3). The peak overpressures at 5 and 7 m included the effect of the reflection and Mach stem. Therefore, P_{TNT} at 5 and 7 m were closer to the MITI87 and NRIPS09 curves, which are for above-ground explo-

Table 3. Numbers of though-holes made by metal fragments.[a)]

	TNT			ETN			PETN		
Distance	3 m	5 m	7 m	3 m	5 m	7 m	3 m	5 m	7 m
Number of through-holes	9	1	1	9	4	3	27	18	4
	3	3	1	6	3	2	25	7	4
	7	3	1	8	1	2	21	11	7
	4	2	2	8	5	3	22	10	4
Average	5.75	2.25	1.25	7.75	3.25	2.5	23.75	11.5	4.75

a) Four steel plates (45 × 60 cm) were used for each distance (0.5, 1.0, and 2.0 m from the explosive center). Average numbers of through-holes in four plates are shown at the bottom of the table.

DOI: 10.1002/prep.201600073

sions (Figure 5). Consequently, the peak overpressure values at 5 and 7 m were used to estimate the TNT equivalent against the MITI87 curve.

ETN showed a much higher level of peak overpressure and an earlier arrival time than TNT at all scaled distances, and was similar to PETN (Figure 2, Figure 3 and Figure 5). The shorter time interval between the first and second wave indicated that the triple point was closer to the sensor (Figure 2 and Figure 4). The TNT equivalents of ETN were slightly higher than that of PETN, although the difference was within experimental error. It was not surprising that the blast parameters of ETN and PETN were similar to each other because they have similar molecular structures. There are a variety of TNT equivalents for PETN, and the value obtained in this study was similar to that in Ref. [22], but higher than that in Ref. [10]. The TNT equivalent can be affected by the scaled distance and scaled height [23, 24]; thus, similar experimental conditions are important for comparing the values of TNT equivalents. In this study, the experiments of ETN, PETN, and TNT were conducted under the same conditions and the peak overpressure of TNT was close to the MITI87 curve. The TNT equivalent of the experimental data of TNT was 1.00 against the MITI87 curve. Therefore, MITI87 was considered to be a reasonable standard curve for these experiments.

The scaled impulse showed similar behavior to the peak overpressure (Figure 5 and Figure 6). The scaled impulse of ETN was slightly smaller than that of PETN, although the peak overpressures of ETN and PETN were almost the same (Table 2). The difference between the peak overpressures and scaled impulse may come from the effect of after-burning and differences in oxygen balance (+5.3% for ETN and −10.1% for PETN), because the after-burning of an oxygen deficient explosive can drive the blast wave for a long time, and consequently increases the impulse [25]; however, the reason was not clear in our work.

In contrast to the peak overpressure, there were significant differences between the fragment velocities of ETN and PETN (Figure 7). The loaded density of the explosives was the main reason for the differences because a high loading density of PETN increases the detonation velocity, and it causes greater fragmentation of the steel cylinder than that of ETN, resulting in a higher fragment velocity of PETN than that of ETN. Thus, the fragment velocity also depends on the loading density, whereas the peak overpressure was related to the energy released or the weight of the explosive. The loaded density of ETN was lower than that of TNT, however, due to its higher power, the fragment velocity of ETN was higher than that of TNT (Figure 7). The number of through-holes increased in the order of PETN, ETN, and TNT (Table 3), which were in good agreement with the results of the initial velocity (V_0).

Fragment velocities were decreased along with the flying distances, suggesting the effect of air resistance on the fragments. From these results, the initial velocities of the fragments were obtained by using the values at 0.5 m, the closest position to the explosion center, where the effect of air resistance was assumed to be smallest. The Gurney constant was calculated for each of the explosives, and the values of TNT and PETN were smaller than some previously reported values [15,26], although the value for PETN was similar to that reported by Künzel et al. [27], which was obtained with low-density powdered PETN. The Gurney constant is affected by the mass ratio, (C/M, where C is mass of the explosive charge, and M is the mass of the metal casing) and the length-to-diameter ratio (L/D) of the explosive and casing [26, 28]. In our experiment, all explosives were powders, and the low loading density resulted in the relatively low C/M ratios (0.41–0.43 for TNT and 0.44–0.45 for PETN), and had low L/D ratios (below 1/1). These experimental conditions explain the relatively low Gurney constants obtained in this study. ETN had lower loaded density ($\rho = 0.71$–$0.73\ g\,cm^{-3}$) compared with PETN ($\rho = 0.88$–$0.89\ g\,cm^{-3}$); therefore, the relatively low detonation velocity of ETN made the Gurney constant lower than that of PETN. Owing to its high sensitivity, ETN cannot be compacted into the cylinder and it has a low loading density. However, ETN has a low melting point (about 61 °C) and it can be melt cast [6], and thus increasing its density may yield different results in future work.

5 Conclusions

The peak overpressure of ETN was much higher than that of TNT, and was similar to that of PETN. The TNT equivalent of ETN was 1.57 under these experimental conditions. The scaled impulse of ETN was higher than that of TNT and slightly smaller than that of PETN. The fragment velocity of ETN was higher than that of TNT, but lower than that of PETN. Gurney constants were calculated from the initial velocity of the fragments.

Acknowledgments

We would like to thank the members of Second Security Division, Security Bureau of the Metropolitan Police Department for help with the field experiments.

References

[1] J. Stenhouse, Ueber die näheren Bestandtheile einiger Flechten, *Justus Liebigs Ann. Chem.* **1849**, *70*, 218–228.
[2] R. Matyáš, M. Künzel, A. Růžička, P. Knotek, O. Vodochodský, Characterization of Erythritol Tetranitrate Physical Properties, *Propellants Explos. Pyrotech.* **2015**, *40*, 185–188.
[3] Q.-L. Yan, M. Kunzel, S. Zeman, R. Svoboda, M. Bartoskova, The Effect of Molecular Structure on Thermal Stability, Decomposition Kinetics and Reaction Models of Nitric Esters, *Thermochim. Acta* **2013**, *566*, 137–148.
[4] M. Künzel, Q.-L. Yan, J. Šelešovský, S. Zeman, R. Matyáš, Thermal Behavior and Decomposition Kinetics of ETN and its Mix-

tures with PETN and RDX, *J. Therm. Anal. Calorim.* **2013**, *115*, 289 – 299.
[5] J. C. Oxley, J. L. Smith, J. E. Brady, A. C. Brown, Characterization and Analysis of Tetranitrate Esters, *Propellants Explos. Pyrotech.* **2012**, *37*, 24 – 39.
[6] V. W. Manner, B. C. Tappan, B. L. Scott, D. N. Preston, G. W. Brown, Crystal Structure, Packing Analysis, and Structural-Sensitivity Correlations of Erythritol Tetranitrate, *Cryst. Growth Des.* **2014**, *14*, 6154–6160.
[7] M. Künzel, O. Němec, R. Matyáš, Erythritol Tetranitrate as a Sensitizer in Ammonium, *Cent. Eur. J. Energ. Mater.* **2013**, *10*, 351 – 358.
[8] V. W. Manner, D. N. Preston, B. C. Tappan, V. E. Sanders, G. W. Brown, E. Hartline, B. Jensen, Explosive Performance Properties of Erythritol Tetranitrate (ETN), *Propellants Explos. Pyrotech.* **2015**, *40*, 460 – 462.
[9] W. E. Baker, *Explosion in Air*, University of Texas Press, Austin, **1973**, p. 150 – 163.
[10] M. M. Swisdak Jr., *Explosion Effects and Properties. Part I. Explosion Effects in Air*, NSWC/WOL/TR 75–116, Naval Surface Weapons Center, Potomac, MD, USA **1975**, 75–116.
[11] C. Kingery, B. Pannill, *Peak Overpressure* vs. *Scaled Distance for TNT Surface Bursts (Hemispherical Charges)*, BRL-1518, Ballistic Research Laboratories, Aberdeen Proving Ground, MD, USA **1964**.
[12] Y. Nakayama, M. Yoshida, Y. Kakudate, M. Iida, N. Ishikawa, K. Kato, H. Sakai, S. Usuba, K. Aoki, N. Kuwabara, K. Tanaka, K. Tanaka, S. Fujiwara, Explosions of Composite Propellants by Ultra-high Pressure Initiation – TNT Equivalences, *Sci. Technol. Energ. Mater.* **1989**, *50*, 88–92.
[13] H. Arai, R. I. Hiyoshi, Blast Pressure Measurement of TNT and Commercial Explosives above the Ground, *Sci. Technol. Energ. Mater.* **2011**, *72*, 1 – 8.
[14] R. W. Gurney, *The Initial Velocities of Fragments from Bombs, Shell and Grenades*, BRL-405, Ballistic Research Laboratories, Aberdeen Proving Ground, MD, USA **1943**.
[15] S. M. Kaye, *Encyclopedia of Explosives and Related Items*, Vol. 10, US Army Armament Research and Development Command, Picatinny Arsenal, **1983**, V63 – V94.
[16] H. Arai, R. I. Hiyoshi, J. Nakamura, Blast Pressure Measurement of Small Charged Powder TNT in a Closed Explosion Chamber, *Sci. Technol. Energ. Mater.* **2011**, *72*, 141 – 146.
[17] R. G. Sachs, *The Dependence of Blast on Ambient Pressure and Temperature*, BRL-466, Ballistic Research Laboratories, Aberdeen Proving Ground, MD, USA **1944**.
[18] T. Matsunaga, T. Aochi, K. Tanaami, M. Iida, K. Miyamoto, A. Miyake, T. Ogawa, Blast Wave Measurements in a Closed Explosion Chamber, *Sci. Technol. Energ. Mater.* **2000**, *61*, 134 – 140.
[19] M. Kudo, M. Kazama, I. Abe, Visualization of Blast Wave by Using its Background and Evaluation of Power of Explosion, *Japanese J. Forensic Sci. Technol.* **2009**, *14*, 93 – 98.
[20] K. M. Leete, K. L. Gee, T. B. Neilsen, T. T. Truscott, Mach Stem Formation in Outdoor Measurements of Acoustic Shocks, *J. Acoust. Soc. Am.* **2015**, *138*, EL522 – EL527.
[21] C. Knock, N. Davies, T. Reeves, Predicting Blast Waves from the Axial Direction of a Cylindrical Charge, *Propellants Explos. Pyrotech.* **2015**, *40*, 169 – 179.
[22] I. Sochet, D. Gardebas, S. Calderara, Y. Marchal, B. Longuet, Blast Wave Parameters for Spherical Explosives Detonation in Free Air, *Open J. Saf. Sci. Technol.* **2011**, *1*, 31 – 42.
[23] M. J. Hargather, G. S. Settles, J. A. Gatto, Optical Measurement and Scaling of Blasts from Gram-Range Explosive Charges, *Shock Waves* **2007**, *17*, 215 – 223.
[24] B. Gelfand, *Blast Effects Caused By Explosions*, N62558–04-M-0004, European Research Office of the U. S. Army, London, UK, **2004**.
[25] R. K. Wharton, S. A. Formby, R. Merrifield, Airblast TNT Equivalence for a Range of Commercial Blasting Explosives, *J. Hazard. Mater.* **2000**, *79*, 31 – 39.
[26] H.-H. Licht, Performance and Sensitivity of Explosives, *Propellants Explos. Pyrotech.* **2000**, *25*, 126 – 132.
[27] M. Künzel, O. Němec, J. Pachman, Optimization of Wall Velocity Measurements Using Photonic Doppler Velocimetry (PDV), *Cent. Eur. J. Energ. Mater.* **2015**, *12*, 89–97.
[28] Y. J. Charron, *Estimation of Velocity Distribution of Fragmenting Warheads Using a Modified Gurney Method*, AFIT/GAE/AA/79S-1, Air Force Institute of Technology, Wright-Patterson Air Force Base, OH, USA **1979**.

Received: March 31, 2016
Revised: August 18, 2016
Published online: ■■ ▮▮, 0000

  DOI: 10.1002/prep.201600073

FULL PAPERS

M. Tagawa, R. I. Hiyoshi, M. Takeuchi, K. Akita*

■■ – ■■

Blast Waves and Fragment Velocities of Erythritol Tetranitrate

DOI: 10.1002/prep.201600073